Low luminosity radio galaxies: effects of gaseous environment

R. Morganti¹, R. Fanti¹, I.M. Gioia^{2,3}, D.E. Harris², P. Parma³, and H. de Ruiter³

- ¹ Dipartimento di Astronomia, Universitá di Bologna, Via Zamboni 33, I-40126 Bologna, Italy
- ² Harvard-Smithsonian, Center for Astrophysics, 60 Garden Street, Cambridge, MA 02138, USA
- ³ Istituto di Radioastronomia, Via Irnerio 46, I-40126 Bologna, Italy

Received February 18, accepted May 19, 1987

Summary. X-ray data from the Einstein Observatory have been collected for a number of low luminosity B2 radio galaxies, in order to study the effect of gas pressure on radio sources. Generally the thermal pressure of the X-ray emitting gas is sufficient to confine most of the radio components. Various possibilities are given for sources where thermal pressure significantly exceeds the non-thermal pressure.

For radio lobes, we find an inverse correlation between the central densities of the cluster gas and the size of the radio structures.

For jets, a study of the pressure ratios is given for different distances from the radio core. In a few cases pressure imbalance is found in the outer regions of the jets. However, from depolarization data, this is unlikely to be produced by a large thermal component inside the radio jets.

Key words: galaxies: radio – X-rays: general

1. Introduction

The possibility that the intergalactic medium plays an important role in the morphologies of radio sources has been considered in a large number of studies.

The external gas can interact with a radio source in different ways: confining the source, modifying its morphology and possibly "feeding" the central engine, i.e. accretion via cooling flows (e.g. Burns et al., 1981).

Radio emitting galaxies can be found in different kinds of environment (rich clusters, poor clusters or groups and also as isolated objects). There is evidence (Harris et al., 1982) that the extended structures of radio galaxies in rich clusters can be confined by the thermal pressure of the surrounding hot gas and, as Burns et al. (1981) pointed out, the same conditions may exist in poor clusters. The detection of X-ray emitting hot coronae (Bechtold et al., 1983; Forman et al., 1985) around early type galaxies has shown that also the hot gas around these galaxies can have characteristics ($T \simeq 1-2 \ 10^7 \ \text{K}$, $n \simeq 1-2 \ 10^{-7} \ \text{cm}^{-3}$) suitable to confine radio components. More questionable is the confinement of powerful radio sources. In the case of Cygnus A (Arnaud et al., 1984) the situation is not clear, because the minimum pressure of the radio lobes is slightly higher than the calculated thermal pressure.

Send offprint requests to: R. Morganti

The amount of detailed structure visible with the new radio telescopes of high sensitivity and resolution has led to a renewed interest in the effects of ambient gas on radio structures. In the present work we address the question of confinement of radio sources by studying twenty-two low luminosity radio galaxies, originally selected from the B2 catalogue, which have been observed with the Very Large Array (VLA) and with the imaging instruments on board the Einstein Observatory. From the radio data we compute the non-thermal pressure within each radio structure. From the X-ray data we estimate the parameters (temperature, density and pressure) of the interstellar and intergalactic gas surrounding the radio components. A comparison is made between the external (thermal) and internal (non-thermal) pressures to determine if the hot gas may effectively confine the radio sources.

2. Description of the sample and data analysis

The B2 sample of low luminosity radio galaxies (Parma et al., 1986; de Ruiter et al., 1986; Fanti et al., 1986, 1987) contains over one hundred objects. In the Einstein Data Bank we have found X-ray observations for twenty-two B2 sources, mainly in clusters of galaxies or B2 sources which are also 3C sources. Therefore the sample of objects studied in this paper is inhomogeneous.

In Table 1 we list the optical and radio properties of the twenty-two galaxies: the B2 name, the redshift of the galaxy, the absolute visual magnitude, the total radio power at 1.4 GHz, the linear size (i.e. a diameter or largest linear dimension) of the radio source in kpc, the NGC name, the cluster name and other radio names like 3C or 4C.

Throughout this paper we will use $H_0 = 100 \,\mathrm{km}\,\mathrm{s}^{-1}\,\mathrm{Mpc}^{-1}$.

2.1. Radio data

The radio observations and data reduction of seventeen radio galaxies in this sample are discussed in Parma et al. (1986), de Ruiter et al. (1986), and Fanti et al. (1986, 1987). For the remaining sources we used published data and maps to determine the radio parameters (see references in Sect. 3, under "Comments on individual galaxies").

The angular resolution of the radio maps is usually much higher than the resolution of the X-ray maps and thus we were able to obtain the non-thermal pressure for different scale structures such as hot-spots, lobes and jets. The non-thermal pressure within a radio feature was calculated using the standard formulas

Table 1. Optical and radio characteristics

B2 name	Z	M_v	$\frac{\log P_{\rm tot}}{({\rm W/Hz})}$	D_r kpc	NGC name	Cluster (group)	Other name
0104 + 32	0.0169	-21.1	24.21	500	383	Arp 331	3C31
0210 + 33	0.0164	-21.8	22.3	31	507	Pisces	_
						Zw. cluster	
0149 + 35	0.0160	-20.2	22.3	16	703	Abell 262	_
0836 + 29	0.0790	-22.4	24.73	331	_	Abell 690	_
0844 + 31	0.0675	-22.2	24.8	270		Zw. cluster	4C31.32
1113 + 29	0.0489	-21.8	24.67	61	_	Abell 1213	4C29.41
1251 + 27	0.0857	-20.9	25.37	50	_	_	3 C 277.3
1303 + 31	0.1816	-22.3	24.39	44	_	Abell 1667	_
1339 + 26	0.0757	-22.6	24.30	194	_	Abell 1775	4C26.41
1346 + 26	0.0633	-22.0	24.55	18	_	Abell 1795	4C26.42
1350 + 31	0.0452	-21.1	25.00	140	-	Zw. cluster	3C293
1502 + 26	0.0540	-21.6	25.86	175	_	Zw. cluster	3C310
1511 + 26	0.1078	-21.0	25.34	212	_	_	3C315
1525 + 29	0.0653	-22.1	23.98	28	_	Abell 2079	_
1553 + 24	0.0426	-21.1	23.36	36	_	_	
1610 + 29	0.0313	-21.2	22.93	60	6086	Abell 2162	_
1615 + 32	0.0296	-20.8	24.30	160	6109	_	3C332
1626 + 39	0.0303	-22.2	24.49	47	6166	Abell 2199	3C338
1657 + 32	0.0631	-21.0	23.65	59	_	Abell 2241 W	4C32.52A
1658 + 32	0.1024	-20.6	23.88	71	_	Abell 2241 E	4C32.52E
1833 + 32	0.0586	-22.1	25.07	133	_	Zw. cluster	3C382
2335 + 26	0.0301	-22.1	24.88	210	7720	Abell 2364	3C465

assuming equipartition between particle and magnetic field energy densities (Pacholczyk, 1970; Fanti, 1982).

Further assumptions are that the radio spectrum can be represented by a power law from 10 MHz to 100 GHz, that the ratio between the energy of electrons and heavy particles = 1, and the filling factor, ϕ , is also = 1.

This last assumption is a significant source of uncertainty because in a few cases there is evidence of filaments in the radio lobes (see Perley et al. (1984) for Cygnus A, and van Breugel and Fomalont (1984) for 3C310). Values for the filling factor <1 can be obtained if the lobes are composed of two types of emitting plasma: high emissivity filaments (not necessarily confined by the external medium) and a diffuse component of low brightness. Usually we do not have the required resolution to determine values of ϕ < 1, but if we use the results obtained for Cygnus A by Perley et al. (1984) we can obtain a rough estimate of the uncertainty introduced by this parameter. The estimated filling factor in Cygnus A is \sim 0.3 -0.03 and with these values we can at least double our estimate of the non-thermal pressure. This will be discussed in more detail in Sect. 4.1.3.

2.2. X-ray data

Data from both imaging instruments (Imaging Proportional Counter, IPC, and High Resolution Imager, HRI) on board the Einstein Observatory (Giacconi et al., 1979) were used in this work.

2.2.1. IPC

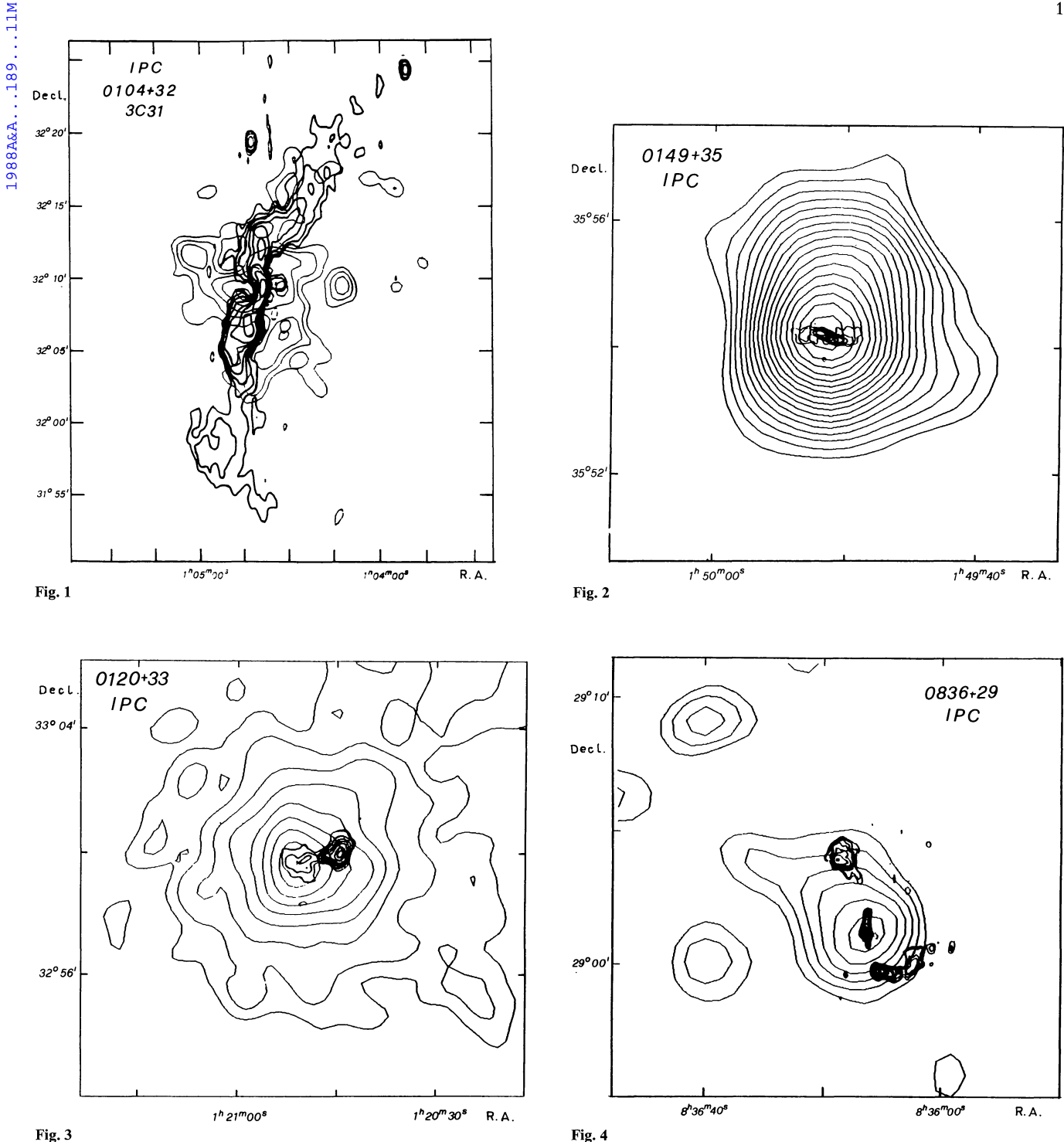
All the IPC images were reprocessed using an improved detection algorithm and background determination (REV1, Harnden et al.,

1984). Twelve of these galaxies belong to Abell clusters and are usually the central galaxies of the cluster. Generally the angular separation between the X-ray centroid and the optical position is less than one arcmin, which is the 3 sigma positional uncertainty of the IPC. With few exceptions the X-ray emission is strong and considerably more extended than the radio emission. Consequently the low brightness radio regions farther away from the core are always embedded in a X-ray emitting hot gas.

Six of the remaining ten objects are either in poor clusters or in groups of galaxies and generally they are the dominant members located in the central regions of the X-ray emission. In these cases the X-ray and radio dimensions are more similar. The final four sources are isolated galaxies; 1615+32 with unresolved X-ray, 1553+24 with weak X-ray emission and two with X-ray upper limits.

2.2.1.1. Maps: In order to examine different scale structures, we constructed X-ray contour diagrams with gaussian smoothing functions of FWHM=60" and FWHM=120" for the IPC data in the energy range 0.5–3.5 keV. Before smoothing, the maps were corrected for vignetting and the background (the mean level in a source free region) was subtracted. The larger gaussian was useful to study the low surface brightness regions. The X-ray contours enabled us to choose the location and radius of circles for intensity and spectral calculations and to estimate source extent either as deconvolved FWHM values or overall (deconvolved) diameters.

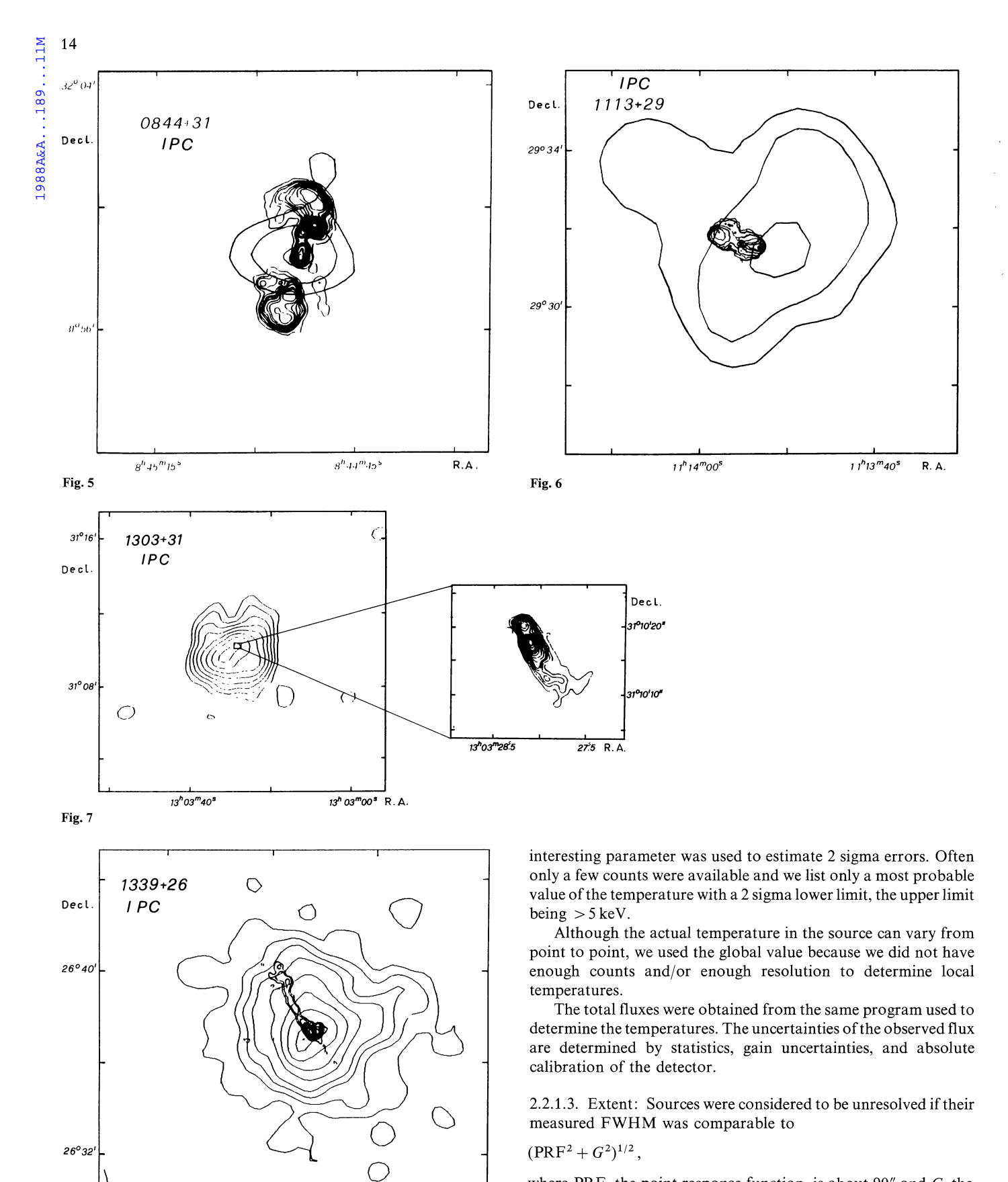
In most cases, we produced X-ray and radio contour diagrams at the same angular scale in spite of the large difference in resolution. This procedure allowed us to select corresponding features in the radio and X-ray for parameter estimation. The radio and the IPC maps are shown overlayed in Figs. 1 through 17.



Figs. 1-17. Radio contour levels superimposed onto X-ray contour maps (IPC). For each source we list in Table 5 the parameters

2.2.1.2. Spectra and fluxes: A rough estimate of the gas temperature was obtained using a standard spectral analysis program (Harnden et al., 1984). This procedure consisted of a least squares fit of the Pulse Height Analysis (PHA) data to various theoretical spectra. We chose the counts within a circle large enough to enclose the 3 sigma contours and subtracted a background calculated from the counts within an external annulus. We assumed thermal bremstrahlung spectra with a

range of temperatures from 0.5 to 7.0 keV and a low energy cut-off derived from 21 cm measurements of the H I column density in our Galaxy (Stark et al., in preparation). These spectral distributions are convolved with the effective area of the telescope and other instrumental filtering to find the expected PHA distribution for the assumed spectra. By comparing the PHA observed distribution with a grid of expected solutions, we find the "best fit" parameters. The method of Avni (1976) for the case of one



where PRF, the point response function, is about 90'' and G, the gaussian smoothing function of the contour maps, was either 60'' or 120''.

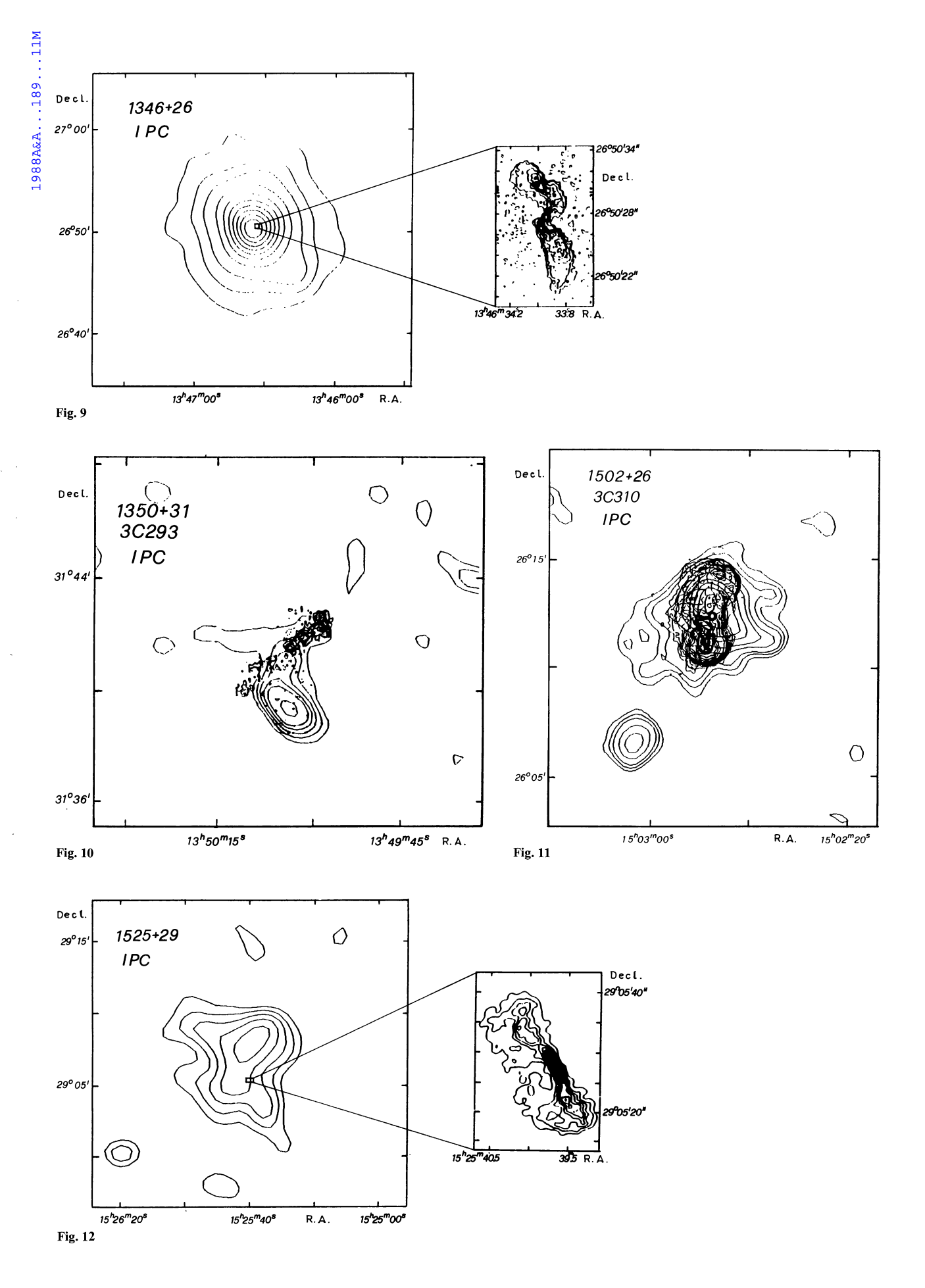
For well resolved sources, deconvolved sizes were measured from the contour diagram as described above. Estimated

R.A.

13^h 39^m20^s

13^h 40^m00^s

Fig. 8



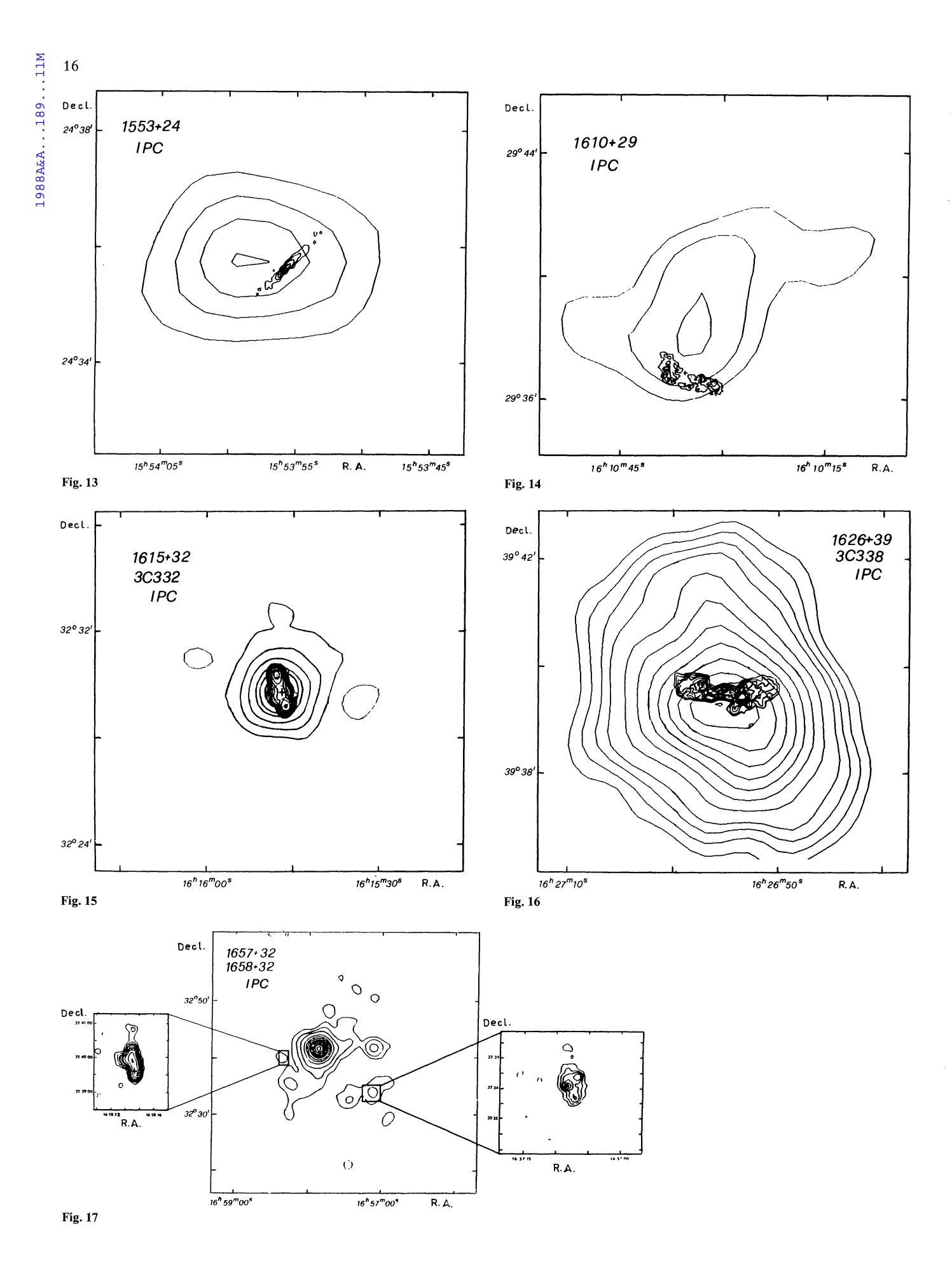


Table 5.

B2 name	(1)	FWHM (2)
0104 + 32	2–5, 7	64
0120 + 33	3, 5, 8, 11, 15, 18, 21, 23, 25	64
0149 + 35	12–27, 29	64
0836 + 29	2-5, 7	120
0844 + 31	3–6	120
1113 + 29	3–5	120
1303 + 31	3–11	64
1339 + 26	3, 5, 6, 8, 10, 12, 14, 16	64
1346 + 26	5, 7, 12, 20, 34, 46, 59, 72, 85, 98, 111	120
1350 + 31	2–7	64
1502 + 26	3-7, 9, 11, 12	64
1525 + 29	3–9	120
1553 + 24	2–5	120
1610 + 29	2–4	120
1615 + 32	2, 6, 9, 12, 14, 16, 18	64
1626 + 39	9, 10, 12–14, 16, 17, 19, 20, 22, 23	64
1657 + 32 $1658 + 32$	2, 4, 6, 11, 14, 17, 21, 25, 27, 29, 31	120

Notes:

(1) Contour levels above the local background in units of sigma (2) The corresponding FWHM in arcsec used for smoothing the X-ray data

uncertainties are of the order of 30% and arise chiefly from statistics and the uncertainty of the spectral distribution (the size of the PRF depends on energy and pulse height channel).

2.2.1.4. Derivation of gas pressure: For the extended sources, with approximately circular shape, we determined the density as a function of radius using a modified King approximation to an isothermal distribution. Following Gorenstein et al. (1978) the X-ray surface brightness distribution is assumed to be

$$S(r) = S(0) \left[1 + (r/a)^2\right]^{-3\beta + 1/2}$$

where a is the core radius and β represents the ratio of the energy per unit mass in galaxies to the energy per unit mass in gas (Cavaliere and Fusco-Femiano, 1976):

$$\beta = \mu m_{\rm H} \sigma^2 / 3 k T_{\rm gas}$$

where μ is the mean molecular weight, $m_{\rm H}$ is the mass of hydrogen atom, σ is the galaxy velocity dispersion and $T_{\rm gas}$ is the X-ray gas temperature. We used a value of $\beta=0.65$ which is appropriate for clusters of galaxies (Jones and Forman, 1984) and measured a=0.65 FWHM.

For irregular structures, the density was calculated also from the surface brightness in the contour diagram. We estimated the emitting volume from the size of the effective beam and the path length through the source, and the density as that required to produce the observed luminosity for a uniform gas filling this volume. In most cases the densities calculated with both methods show good agreement (difference < 30 %). In every case the values found with the last method are compatible with the range or limit in density obtained with the first one.

Another uncertainty in calculating the density at any point in an extended source comes from the difficulty in properly estimating the core radius. Jones and Forman (1984) demonstrated the existence of central X-ray excesses in the X-ray surface brightness profiles of many clusters. If similar excesses are present in the objects under study (see Sect. 3) they may not have been noticed since our data might not have the required angular resolution. This will lead to an underestimate of the core radius, an overestimate of the central density and an error in the calculation of density as a function of radius.

The thermal pressure at any location within the X-ray source is taken $\sim 2n kT$. The uncertainty in the pressure can be estimated from the functional dependence of the pressure on the observed quantities:

$$P \simeq (F_x^{1/2} T^{3/4})/(D^{1/2} \theta^{3/2}),$$

where F_x is the flux, T the temperature, D the distance and θ the angular scale.

For typical uncertainties of the order of 30 % in F_x , 30 % in θ , and a factor of two in T, the contributions to the uncertainty in the pressure are the following factors: 1.14, 1.5, and 1.7. Thus the total error to the pressure is roughly a factor of three.

The thermal pressure should be considered as an average value across a region corresponding to the angular resolution and one must remember that regions with higher gas pressure may be present for small scale features which we were unable to resolve.

Table 2 lists the IPC parameters: in column 1 the B2 name and the IPC number, in column 2 the X-ray flux in the 0.5-3.5 keV band in unit of $10^{-12} \,\mathrm{erg}\,\mathrm{cm}^{-2}\,\mathrm{s}^{-1}$ (the global flux errors are estimated to be approximately 30% at 2σ when few counts are present, and somewhat better for stronger sources); in column 3 the most probable value for the gas temperature in keV and, in parenthesis the corresponding 2σ error (if the upper limit is above 5 keV we only give the lower limit to the value of the temperature, see also 2.2.1.2); in column 4 the X-ray luminosity in 10^{42} erg s⁻¹; in column 5 the most probable value for the central density of the gas in 10⁻³ cm⁻³ (obtained using the modified King approximation) and, in parenthesis the corresponding 2σ error (obtained from the temperature error); in column 6 the core radius in arcsec (two different values are given when the core shows an evident elliptical structure) and finally in column 7 the linear size (diameter) of the X-ray emitting gas in kpc.

2.2.2. HRI

For the HRI data the FWHM of the gaussian smoothing function ranges between 7'' and 20''. For six objects HRI data were analyzed. Three objects (0104+32, 1833+32 and 2335+26) are unresolved and the X-ray source coincides with the radio core suggesting the presence of nuclear activity. In fact, for the sources 0104+32 and 2335+26 the HRI flux represents only a small fraction of the total source flux obtained from IPC data. In the case of 1833+32 also the IPC shows an unresolved source. The remaining three objects (0149+35, 1346+26 and 1626+39) show extended X-ray emission. In these objects Jones and Forman (1984) found a central excess in the brightness distribution of the IPC emission, which they attribute to a cooling flow.

The parameters derived from the HRI are summarized in Table 3. They are: the X-ray flux in the $0.1-4.5\,\mathrm{keV}$ band in units of $10^{-12}\,\mathrm{erg\,cm^{-2}\,s^{-1}}$ obtained assuming a thermal bremstrahlung spectrum with two different values for the temperature; the linear size (diameter) of the X-ray emitting region in kpc; the central density of the gas in $10^{-3}\,\mathrm{cm^{-3}}$ and the thermal pressure, P_{th} in $10^{-12}\,\mathrm{dyne\,cm^{-2}}$.

The density was calculated only for the three galaxies with extended HRI emission using the surface brightness as described

Table 2. IPC parameters

Source name	Flux 10 ⁻¹² erg cm ⁻² s ⁻¹	kT (keV)	$L_{\rm x}$ $10^{42} {\rm erg s^{-1}}$	$\frac{N_{\rm c}}{10^{-3} {\rm cm}^{-3}}$	a (arcsec)	D_x (kpc)
0104 + 32	2.0	3.0	0.6	1.5	224	142
I 6308		(>1.0)		(< 2.5)		
0120 + 33	7.8	2.5	2.2	6.6	123	140
17766		+1.2/-0.7		+0.7/-0.9		
0149 + 35	21.0	2.2	5.7	12.0	123	150
1295		+1.1/-0.7		+1.9/-1.6		
0836 + 29	0.6	1.9	4.2	0.9	150	350
16020		(>0.5)		(<1.7)		
0844 + 31	0.3	> 0.5	1.4	< 2.0	_	60
I3918				. .		
1113 + 29	1.3	6.0	3.4	2.4	110	250
I1844	0.0	(>1.5)	•	(<3.0)	220	
1251 + 27	< 0.3		< 2.6	< 3.4	-	_
I3917	2.0	4.0	00.0	2.2	0.0	200
1303 + 31	3.0	4.0	80.0	2.2	80	290
12046	7.4	+2.0/-3.0	45.0	+2.4/-0.1	110	500
1339 + 26	7.1	6.0	45.0	2.6	150	500
I320	40.5	(>4.0)	212.0	(<2.7)	150	400
1346 + 26	48.5	6.5	212.0	5.9	150	480
I293	0.22	(>6.0) >0.5	0.5	(<6.0)	190 90	125
1350 + 31 16327	0.23	>0.3	0.3	< 3.5	90	125
10327 $1502 + 26$	1.3	0.6	4.1	1.5	123	310
I 1907	1.3	(>1.5)	4.1	(<2.2)	123	310
1517 + 26	< 0.1	(>1.5)	< 1.3	<1.1		
I1909	V 0.1		\ 1.3	\1.1		_
1525 + 29	2.3	7.0	11.0	1.5	150	413
I1854	2.3	(>1.5)	11.0	(<3.0)	200	713
1553 + 24	0.2	6.0	4.2	3.9	90	70
I4950	0.2	(>0.5)	1.2	(<11.0)	70	, 0
1610 + 29	0.7	6.0	0.8	1.4	95	105
I1856	· · ·	(>0.5)	3.0	(<4.0)	175	100
1615 + 32	1.0	1.9	27.0	<0.8a	-	100
I6319		(>0.5)				
1626 + 39	43.01	<1.0	43.0	>9.4	170	290
I 2691					214	
1657 + 32	< 0.2		< 0.5	<1.3 a		_
14954						
1658 + 32	< 0.1	_	< 1.0	<1.6a	_	_
I 4954						
1833 + 32	12.7	4.0	45.0	< 2.8 a	-	< 150
12650		+3.0/-2.0				
2335 + 26	6.0	2.5	5.7	2.4	170	400
I8356		(>1.5)		(< 2.7)	300	

^a Thermal density at radio source position

in Sect. 2.2.1.4. The radio and HRI maps are shown overlayed in Figs. 18 through 21.

3. Comments on individual sources

0104+32 (3C31) (Fig. 1): This well studied radio source (Fomalont et al., 1980; Strom et al., 1983) is associated with the

bright galaxy NGC 383, which is the dominant member of a chain (Arp 331). The radio observations show a two sided jet which broadens away from the central component, merging gradually into low brightness regions. The radio map reproduced in Fig. 1 is taken from Strom et al. (1983). The straight parts of the jets are inside the X-ray emission whereas the low brightness extensions (both to the north and to the south) lie mostly outside the X-ray emission. From the HRI data we detected only an unresolved source coincident with the radio core.

Table 3. HRI parameters

Source	Flux $10^{-12} \text{erg cm}^{-2} \text{s}^{-1}$		D_x (kpc)	$N_{\rm C}$ $(10^{-3} {\rm cm}^{-3})$	$P_{\rm th}$ 10^{-12} dyne cm ⁻²
	kT=1	kT=5			
0104 + 32	0.2	0.4	Point	_	_
0149 + 35	1.9	3.2	14	15 $(kT=1)$	42 - 28
1346 + 26	17.0	31.0	100	21(kT=5)	270
1626 + 39	31.0	54.0	60	25(kT=1)	72 - 39
1833 + 32	11.0	19.0	Point	_ ` ′	_
2335 + 26	0.1	0.2	Point		

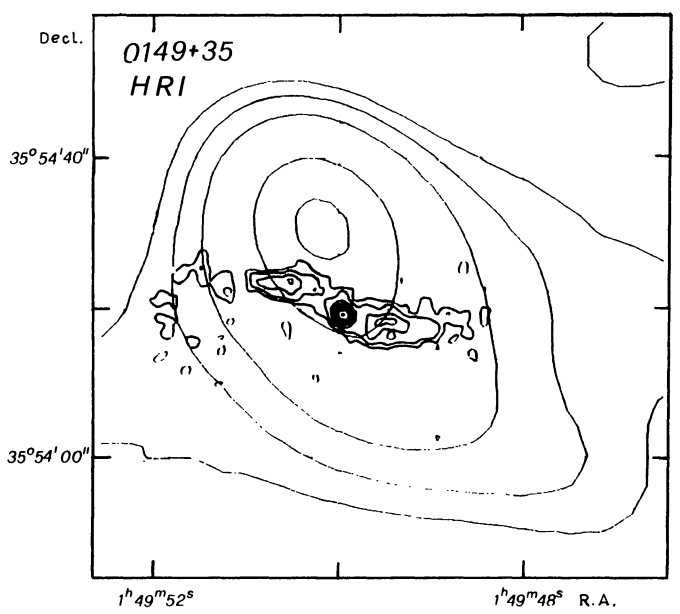


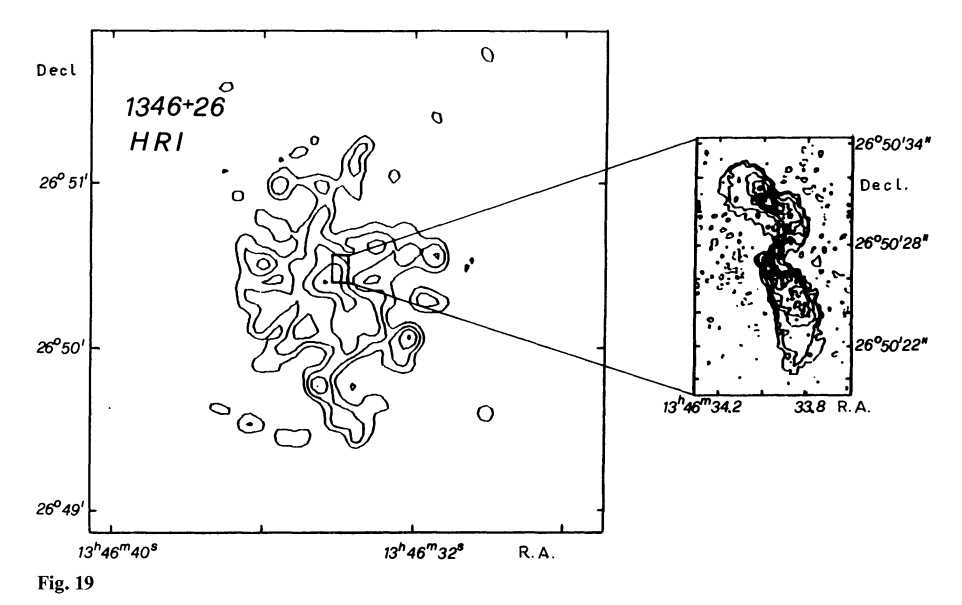
Fig. 18

0120+33 (Fig. 2): This galaxy (NGC 507) is the brightest object in the Pisces group. The two lobes are faint with a very steep radio spectrum (spectral index ~ 1.4) (Colla et al., 1975).

0149+35 (Figs. 3 and 18): This is the brightest galaxy (NGC 708) in Abell 262. Jones and Forman (1984) found a central excess in the brightness distribution of the IPC emission, which they attribute to a cooling flow. The small scale X-ray structure (HRI data) is extended (>10 kpc) and asymmetric. The peak of the X-ray emission is not coincident with the radio core and the optical object.

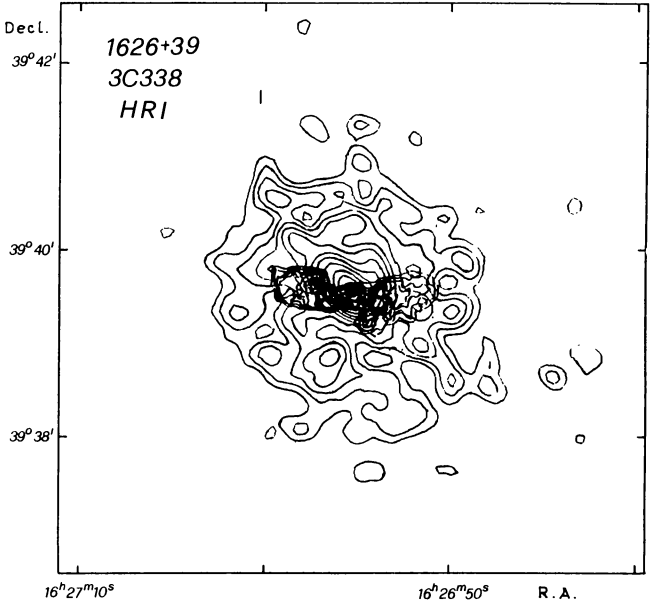
0836+29 (Fig. 4): This radio source is associated with the brightest galaxy in Abell 690. The narrow, linear radio structure (northern jet) lies within the high brightness X-ray region and both southern and northern radio lobes lie at the edge of the IPC emission

0844+31 (Fig. 5): If the X-ray emission is actually extended, this would be a beautiful example of an abrupt change in radio morphology between the structure inside the X-ray emission



Figs. 18-21. Radio contour levels superimposed onto X-ray contour maps (HRI). For each source we list in Table 6 the parameters

20





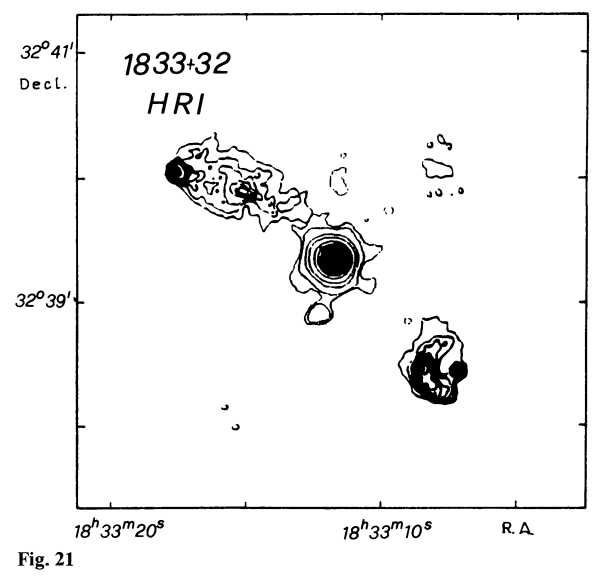


Table 6.

B2 name	(1)	FWHM (2)
0149 + 35	3–7	20
1346 + 26	3–8	7
1626 + 39	3–15	13
1833 + 32	2, 3, 6, 9, 15, 21, 27, 33, 39, 45, 51, 57	7

Notes:

(1) Contour levels above the local background in units of sigma (2) The corresponding FWHM in arcsec used for smoothing the X-ray data

- (narrow, linear) and the extended parts (low brightness, diffuse radio structure). The radio map reproduced in Fig. 5 is taken from Machalski and Condon (1985). Unfortunately few counts are available and the X-ray emission may be unresolved, i.e. it could originate from nuclear activity.
- 1113+29 (Fig. 6): This radio source is associated with the northern galaxy of a double system in the center of Abell 1213 and shows a one sided jet, which is more evident when observed at higher resolution (Fanti et al., 1986). Also in this case few counts are available for the X-ray emission.
- 1251+27: The radio source 3C277.3=Coma A (Bridle et al., 1981a) presents a double structure with wide radio lobes. Only an upper limit is available for the X-ray emission. No map is shown.
- 1303+31 (Fig. 7): This radio source is associated with the brightest galaxy in Abell 1667 (Coma B) and shows a head-tail structure. Radio and X-ray dimensions are too different for overlaying the two maps.
- 1339+26 (Fig. 8): This radio source is associated with a close pair of galaxies in Abell 1775 (O'Dea and Owen, 1985; Parma et al., 1986): a head-tail and a wide angle tail source which are not separated in the present map. The head of the first galaxy is almost coincident with the X-ray center while the tail moves away radially from the center.
- 1346+26 (Figs. 9 and 19): The radio source is much smaller than the IPC X-ray size. The radio emission is associated with the cD galaxy in Abell 1795. The radio map reproduced here is taken from van Breugel et al. (1984). The IPC emission shows a central excess (Jones and Forman, 1984) probably associated with a cooling flow. Also the HRI emission is more extended than the radio image.
- 1350+31 (Fig. 10): This radio source (3C293) has a broad emission bridge terminating in a hot-spot (the map reproduced here is taken from Bridle et al., 1981 b) and lies north of the main X-ray emission.
- 1502+26 (Fig. 11): The radio source, 3C310 (the radio map reproduced in Fig. 11 is taken from Leahy and Williams, 1984), lies in a Zwicky cluster (Burns and Gregory, 1982) and is mainly composed of two large and diffuse lobes. The radio lobes show evidence of shells and filaments in the high resolution maps (van Breugel and Fomalont, 1984).
- 1511+26: The radio structure of 3C315 is double lobed (Leahy and Williams, 1984). Only an upper limit is available for the X-ray emission. No map is shown.
- 1525+29 (Fig. 12): The double jet radio source is associated with the fainter southern galaxy of a double system in a common halo and is located at the center of Abell 2079. The radio and X-ray sizes are too different for a direct overlay.
- 1553+24 (Fig. 13): The radio emission shows a typical example of a "lobeless" jet. No evidence of lobes is found with the present brightness sensitivity. The X-ray emission is weak with only a few counts available.

1610+29 (Fig. 14): This source is associated with the brightest galaxy (NGC 6086) in Abell 2162. The radio emission is faint and shows two "relaxed" lobes. The offset between the radio and the X-ray centroid seems to be larger than the positional error of the IPC.

1615+32 (Fig. 15): This is an isolated object (3C332) which shows a double radio structure. The X-ray emission is unresolved and could originate from nuclear activity.

1626+39 (Figs. 16 and 20): This is the brightest member (NGC 6166) of Abell 2199. The radio emission is quite complex (Burns et al., 1983). Jones and Forman (1984) found a central excess in the IPC brightness distribution associated with a cooling flow. The HRI emission is extended and shows a peak coincident with the radio core.

1657+32/1658+32 (Fig. 17): These radio galaxies belong to two different clusters (Abell 2241 East and Abell 2241 West) projected onto each other (Bijleveld and Valentijn, 1982). The prominent X-ray source in the field is associated with the D galaxy in A2241 E and also with a radio galaxy in A2241 W. 1657+32 is a member of Abell 2241 W (z=0.06) while the head-tail 1658+32 (O'Dea and Owen, 1985) is a member of Abell 2241 E (z=0.102).

1833+32 (Fig. 21): This source (3C382) shows a structure typical of high luminosity radio sources: i.e. two lobes with hotspots. Both the IPC and HRI sources are unresolved and they have almost the same flux.

2335+26: This wide angle tail source (3 C 465-NGC 7720) lies in Abell 2364. The radio and X-ray emission were studied in detail by Eilek et al. (1984). The HRI observation shows a point source coincident with the radio core. No map is shown.

4. Results and discussion

Three objects, 0844+31, 1615+32, and 1833+32, appear to be unresolved in the IPC images. In the case of 1833+32 this is

confirmed by HRI data, which show a point source with a flux similar to IPC flux. In all three cases the X-ray emission is centered on the radio core and may therefore originate from the nuclear activity rather than thermal bremstrahlung from an ambient gas.

The X-ray surface brightness of the lowest contour was used to infer an upper limit for the thermal density and pressure around the radio lobes.

Because of the low resolution and the large positional uncertainty of IPC data, it is difficult to study positional anticoincidences between radio and X-ray emission (e.g. prevalence of radio emission in regions where the X-ray emission is faint or absent) as an effect of the buoyancy from the pressure gradient. This effect has been considered in detail in different studies, in particular for the cases of tailed sources (see e.g. Burns and Balonek, 1982).

In Fig. 22 we plotted the linear size (D_r) of each radio source against the most probable value of the central density (N_c) as determined from the X-ray observations. Both parameters appear correlated: high values of N_c are found in small radio sources, while the more extended radio sources are associated with galaxies located in a medium with a low central density. In fact, a linear regression of $\log(D_r)$ on the logarithm of the most probable value of the central density (N_c) , taking into account the upper limits (as described by Avni, 1976), gives $D_r \sim N_c^{-1.2}$. We also considered the well-known dependence of D_r on radio power P (see, e.g., Ekers et al., 1981). We tried multiple regression of $\log(D_r)$ on both $\log(N_c)$ and $\log(P)$; the resulting correlation gives a very weak dependence on P (exponent ~ 0.15) and a small change in the exponent of $N_c (\sim -1.0)$.

In view of the large uncertainties associated with N_c and the few points in the diagram, the exact form of the regression should be taken with caution; we believe that a more detailed analysis is, at this point, unwarranted. However, we consider the correlation between D_r and N_c to be an indication that cluster gas has a direct influence on the morphology of a radio source. Moreover, from the present data, the linear radio size is close to inversely proportional to the central gas density, and this is precisely the dependence one naively would expect (for example in the "independent blob" model of Jaffe and Perola, 1974).

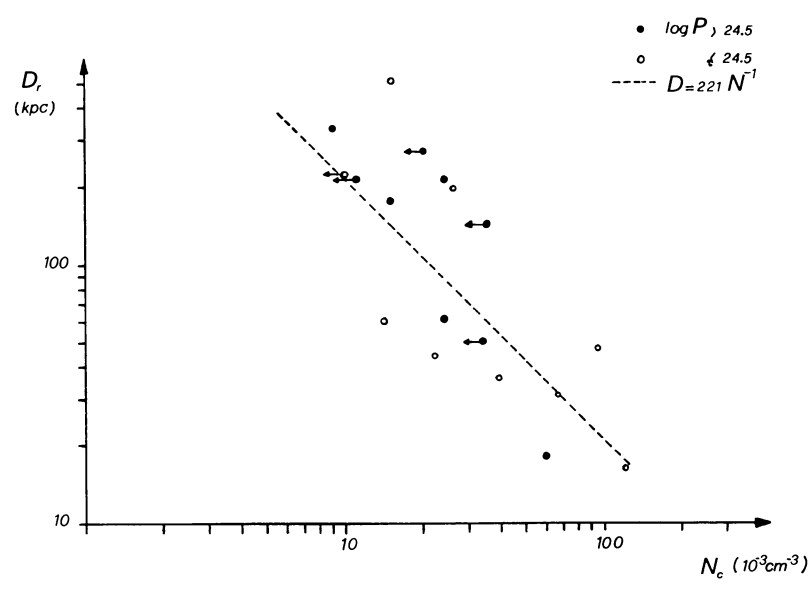


Fig. 22. Plots of radio dimensions of the sources versus the central density of the X-ray emission

Table 4.

Source		d (arcsec)	$P_{\rm th}$ 10^{-12} dyne cm ⁻²	$P_{n \text{th}}$ P_{th}	$/P_{n \mathrm{th}}$
0104+32	N jet	600 360 200 30 30	1.7(>1.0) 3.9(>2.1) 7.6(>4.2) 13.2(>7.2) 13.2(>7.2)	13.8 1	
	Š	150 360 660	9.4(>5.2) 3.9(>2.1) 1.7(>1.0)	~ 0.5 7	.4 .8 .5
0120 + 33	E lobe W lobe	40 28	$40.0 (\pm 12)$ $46.0 (\pm 12)$	3.6 11 6.5 7	.1 .1
0149 + 35	E jet W jet	12 2 2	72 (+25/-18) 73 (+25/-18) 73 (+25/-18)	75.0 1 75.0 1	.8 .0 .0
0836+29	jet N lobe S lobe S lobe	12 8 40 180 95 120	72 (+25/-18) $5.2 (> 3.0)$ $4.9 (> 2.8)$ $2.2 (> 1.3)$ $3.8 (> 2.2)$ $3.2 (> 0.9)$	34.0 0 6.0 0 0.5 4 1.5 2	.2 .2 .8 .4 .5 .3
0844+31	N jet N lobe S lobe	25 63 ~100 ~100	< 8.3 < 8.3 < 1.0 < 1.0	9.0 < 0 2.3 < 3 0.3 < 3 0.4 < 2	.6 .3
1113 + 29	jet E lobe	7 23 33	19.0 (>8) 18.6 (>7.6) 18.0 (>7.0)	25.0 0	.3 .7 .6
1251 + 27	hot spot N lobe knots S lobe	20 12 ~ 8 15	<20.0 <20.0 <20.0 <20.0	$\begin{array}{rrr} 130.0 & < 0 \\ 17.0 & < 1 \\ 160.0 & < 0 \\ 25.0 & < 0 \end{array}$.2 .1
1303 + 31	head tail	9	27.6 + 15/ - 14 27.6 + 15/ - 14		.2 .6
1339 + 26	head tail	20 150	40.0 (>28) 39.0 (>28) 20.0 (>14)		.6 .2 .3
1346+26	N jet S jet	4 4	108.0 (>98) 108.0 (>98)		.8–1.6 .7–1.9
1350+31	bridge hot spot	14 60 90	> 5.4 > 3.8 > 3.8	5.0 1 4.9 0 11.0 0	.8
1502 + 26	N lobe S lobe	120 100	14.6 (>5.3) 17.1 (>6.2)	1.7 8 2.8 6	.6 .1
1511 + 26	S lobe N lobe	60 60	< 6.1 < 6.1	3.0 < 2 3.9 < 1	
1525 + 29	N jet S jet	8 5	27.0 (>8.9) 27.0 (>8.9)		.8 .4
1553 + 24	N jet S jet	20 5 5 10	68.0 (>15) 71.0 (>16) 71.0 (>16) 71.0 (>16)	3.6 19 18.0 3 17.5 4 4.2 17	.9 .1

Table 4 (continued)

Source		d (arcsec)	$P_{\rm th}$ $10^{-12} { m dyne cm^{-2}}$	$P_{n \mathrm{th}}$	$P_{ m th}/P_{n m th}$
1610 + 29	W lobe E lobe	35 60	24.3 (> 5.6) 21.1 (> 4.9)	0.8 1.2	30.4 17.6
1615 + 32	N lobe S lobe	35 35	< 7.5 < 7.5	9.0 6.4	0.8 1.2
1626+39	W lobe E lobe	46 22 17 26 40	24.0 (<35) 24.0 (<35) 24.0 (<35) 24.0 (<35) 24.0 (<35)	8.0 27.0 39.0 14.0 8.0	3.0 0.9 0.6 1.7 3.0
1657 + 32			< 6.6	4.0	< 1.7
1658 + 32	head tail	30	< 4.6 < 4.6	7.0 1.0	< 0.7 < 4.6
1833 + 32	S lobe N lobe N lobe	70 53 70	<10.3 <10.3 <10.3	12.8 8.4 4.2	< 0.8 < 1.2 < 2.5
2335 + 26	NS tail	150 90	11.8 (>7.8) 15.2 (>10)	4.9 8.5	2.4 1.8
	EW tail	44 110 233	17.5 (>11) 15.2 (>10) 7.9 (>5)	14.7 6.9 2.9	1.2 2.2 2.7

4.1. Comparison of thermal and non-thermal pressure

4.1.1. Assumptions for pressure balance

In Table 4 we present, for various distances (d) from the radio core the most probable value for the thermal pressure, $P_{\rm th}$ (and, in parenthesis, the corresponding 2σ error) obtained from the IPC data (see Sect. 2.2), the non-thermal pressure, $P_{\rm nth}$, and the ratio between these two pressures ($P_{\rm th}/P_{\rm nth}$) determined using the most probable value of $P_{\rm th}$. Wherever a range of $P_{\rm nth}$ is given, it represents the values found closest and farthest from the radio core.

Several uncertainties which limit the accuracy in the calculations of thermal to non-thermal pressures have already been mentioned (Sect. 2.2.1.4). Furthermore the absolute position from the IPC has a 90% confidence uncertainty of about 30". This means that, when making a comparison between a radio component and the brightness of the X-ray emission, errors may occur in calculating the thermal pressure in locations where the X-ray intensity is changing rapidly. The severity of this effect is mitigated somewhat by the low resolution of the IPC which effectively smooths rapid density variations. Only in the cases of clumpy X-ray emission will the pressure errors be dominated by the positional uncertainty. This problem is much less severe for the HRI, where the 90% confidence uncertainty in position is of the order of 4".

The low resolution of the IPC precludes us from recognizing small scale, high density regions. This means that the actual pressure of the gas surrounding radio features may be much greater than the large scale average that we calculated. Finally we have to be aware of projection effects. For the purpose of our calculation we have tacitly assumed that the radio source is actually embedded within the hot gas and lies at the point of highest density along the line of sight. Thus the actual thermal pressures could be lower than those calculated if the radio component is in front of or behind the assumed location.

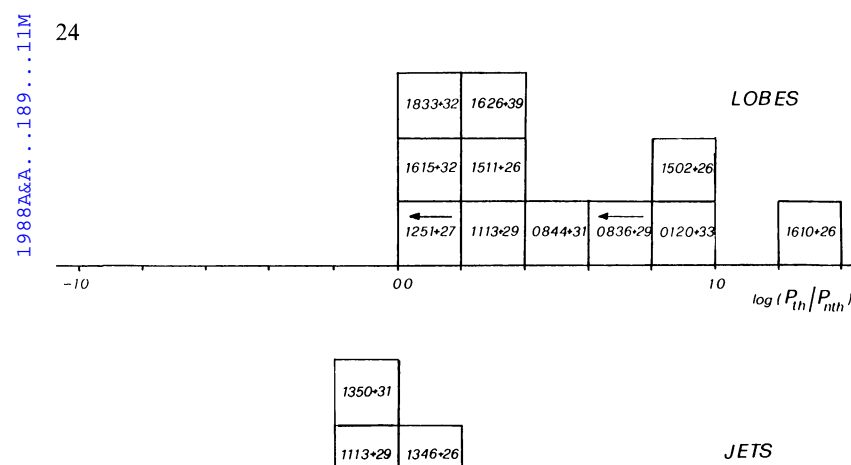
For most sources the two pressures are similar, especially if one considers the large uncertainties associated with both parameters. As a working hypothesis, we assume the external and internal gas to be in equilibrium if the thermal and non-thermal pressures are equal to within a factor of three. If the ratio is greater than six, the external and internal gas are considered to be out of equilibrium. Values between three and six give only marginal evidence of imbalance.

4.1.2. Sources with $P_{th} > P_{nth}$

In three sources (0120+33, 1502+26, and 1610+29) the thermal pressure greatly exceeds the non-thermal pressure by a factor >6 over the whole source. It is difficult to explain this excess solely on the basis of observational errors, even if allowance is made for large uncertainties in some parameters.

A partial imbalance is found in the tail of 1339 + 26: the non-thermal pressure is much lower than the pressure of the surrounding medium. However, in this case projection effects may be important. Assuming a reasonable length for the tail (600 kpc) and an angle of 15 degrees between the tail and the line of sight, the pressure imbalance can in part be reduced $(P_{\rm th}/P_{\rm nth} \sim 6)$ because much of the tail would actually lie outside the observed X-ray distribution.

Sometimes the ratio of thermal to non-thermal pressure increases with the distance from the radio core (e.g. 0104+32). In order to emphasize this effect, the results of Table 4 are visualized in two histograms (Figs. 23a and b), which show the distribution



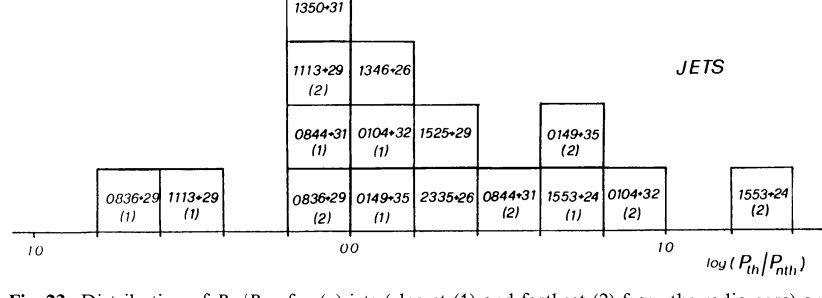


Fig. 23. Distribution of P_{th}/P_{nth} for (a) jets (closest (1) and farthest (2) from the radio core) and (b) for the lobes

of $P_{\rm th}/P_{\rm nth}$ for jets and lobes. When possible, two values for this ratio along the jets (closest (1) and farthest (2) from the radio core) are shown. Although this may reflect an actual progression from equilibrium to non equilibrium, the observed effect may be artificially introduced by the large difference in resolution between the X-ray and radio beams. If small scale gas features of high density are present, they would not be recognized as such with the low resolution of the IPC. Thus $P_{\rm th}/P_{\rm nth}$ could be underestimated close to the core.

4.1.3. Possible reasons for $P_{\rm th} > P_{n\rm th}$

There are three general considerations which could explain the apparent pressure imbalance. The first of these is the departure from the minimum pressure condition: a) if the magnetic field strength is significantly different from the equipartition value, the total non-thermal pressure will be greater than the calculated value; b) similarly the total pressure would increase if there were a large number of "uncounted" electrons (i.e. a significant contribution to the radio luminosity outside the 10 MHz to 100 GHz band); c) a significant contribution to the total energy from protons or other cosmic ray particles and d) a small filling factor. As van Breugel and Fomalont (1984) pointed out, in some low luminosity radio galaxies surrounded by a relatively high density medium, much of the energy coming from the nucleus may be associated with the formation of "bubbles". This scenario was partially confirmed by the discovery of filaments in the high resolution map of 3C310. This fact suggests that the filling factor can have large deviations from unity: a filling factor around 0.02-0.05 is needed to increase the non-thermal pressure of the above mentioned sources to about the thermal pressure of their surrounding (cf. $\phi = 0.3$ to 0.03 for Cygnus A).

The second consideration is the possibility that a large thermal component inside the radio source might give a significant contribution to the internal pressure. The steep spectral index and the "relaxed", faint radio emission found for 0120 + 33 and 1610 + 29 suggest that they could be old sources, in which the nuclear

activity is turned off. Thus, the thermal component inside the radio source may have become dominant due to the mixing of the internal and external medium.

Finally, as mentioned above, due to projection effects the radio components may not actually be within the gas that gives rise to the X-ray emission.

4.1.4 Pressure balance for jets

A large number of sources in our sample show jet structures. A detailed study of the whole B2 sample can be found in Parma et al. 1987 where a number of parameters for the jets are derived. For each source the FWHM is measured as a function of the angular distance from the radio core to derive the opening angle of the jet (this was done by making cross cuts in the direction perpendicular to the jet orientation). Furthermore the variation of surface brightness with the jet width was calculated along the jet. Using these parameters we have calculated the non-thermal pressure in different positions along the jet.

Generally, the agreement between this pressure and the static pressure (or an upper limit) of the external medium is satisfactory. Low ratios of $P_{\rm th}/P_{\rm nth}$ in regions close to the radio core are not necessarily indicative of a pressure imbalance, since the dimensions of the jet close to the core are not well determined. On the other hand, such an overpressure may well be real, since it may be impossible to confine statically the first part of a jet (cf. other compact structures like knots and hot-spots). Along the jet we found that the ratio between external and internal pressure increases with distance from the core. As mentioned above this can be an effect of the large difference in resolution between the two observations; alternatively it would be necessary to invoke a large thermal component inside the radio jets.

In order to estimate the average density of an internal thermal component, we have used the polarization data (Morganti et al., 1987). For two sources of the present sample (1113 \pm 29, 1553 \pm 24), we could set upper limits to the thermal density inside the radio source (assuming that depolarization, if any, is due to

internal Faraday rotation and that the magnetic field along the line of sight in the jet does not have many field reversals).

The thermal densities in the jets are always lower than the density of the external gas ($\varrho_{\rm jet}/\varrho_{\rm ext}\sim 0.1-0.5$), so that, for them, the presence of a large thermal component is excluded.

This result is in agreement with the current scenario describing the jets in FRI radio sources. Such jets seem to have a low Mach number (Morganti et al., 1987) and need a small ratio between the internal and external thermal gas density (0.1–0.01 Bicknell, 1985). Under these conditions, buoyancy may play a significant role in the dynamics of a jet.

5. Conclusions

We have studied the problem of confinement of radio galaxies using VLA and Einstein observations of 22 low luminosity radio galaxies (belonging to the B2 catalog). Most of these sources are in clusters or groups and only three objects appear to be unresolved in the IPC images.

From the X-ray data we have derived the density and the pressure of the hot intergalactic (or interstellar) medium as a function of distance from the nucleus. Using the radio data we obtained the non-thermal pressure inside the radio sources. In spite of the large uncertainties in the determination of these parameters, some interesting results can be emphasized:

i) Perhaps the most striking result of our investigation is that very often the external and internal pressure are in equilibrium. This is less trivial that it may seem, since the uncertainties in the determination of thermal and non-thermal pressure are large and, moreover, both were calculated independently.

The pressure equality is in agreement with the idea of a radio source evolving towards a situation of equilibrium, by adapting its internal pressure (via expansion) to the pressure of the external medium. It appears therefore that for this class of low luminosity radio sources the non-thermal pressure (minimum pressure) can be used to provide an estimate of the external gas pressure.

- ii) In a few cases the external pressure seems significantly larger than the "equipartition pressure". While this could be due to a deviation from equipartition conditions, we note that it happens in objects which seem to be old radio remnants (0120 \pm 33, 1610 \pm 39, 1502 \pm 26, the tail 1339 \pm 26). It is possible that a considerable mixing of the radio lobes with the external medium has taken place and that most of the internal pressure is now provided by thermal material. An alternate possibility is that these sources have a filamentary structure (as in the case of 3C310) so that the non-thermal pressure is larger by an order of magnitude than the minimum (equipartition) pressure.
- iii) The presence of a link between the radio source morphology and the characteristics of the environment is also confirmed by the fact that a correlation is found between the dimension of a radio source and the central density derived from the X-ray emission (see Fig. 22). This indicates that the distribution of the interstellar or intergalactic medium affects the morphologies of radio structures.

Acknowledgements. We would like to thank G. Fabbiano for useful discussions and critical comments, which improved the manuscript and C. Stern for assistance in preparing the X-ray maps. R.M. acknowledges the support from the Smithsonian Institution under the Short Term Visitor program at the CfA, where part of this work was performed. She thanks

H. Tananbaum for the kind hospitality. This work has received partial financial support from NASA contract NAS 8-30751.

References

Arnaud, K. A., Fabian, A. C., Eales, S. A., Jones, C., Forman, W.: 1984, Monthly Notices Roy. Astron. Soc. 211, 981

Avni, Y.: 1976, Astrophys. J. 210, 642

Bechtold, J., Forman, W., Giacconi, R., Jones, C., Schwarz, J.,
Tucker, W., Van Speybroeck, L.: 1983, Astrophys. J. 265, 26
Bicknell, G.V.: 1985, Proc. Physics of Energy Transport in Extragalactic Radio Sources, eds. A.H. Bridle, J.A. Eilek, p.

Bijeleveld, W., Valentijn, E. A.: 1982, Astron. Astrophys. 111, 50 Bridle, A.H., Fomalont, E.B., Palimaka, J.J., Willis, A.G.: 1981a, Astrophys. J. 248, 499

Bridle, A.H., Fomalont, E.B., Cornwell, T.J.: 1981b, *Astron. J.* **86**, 1294

van Breugel, W., Heckman, T., Miley, G.: 1984, Astrophys. J. 276, 79

van Breugel, W.J.M., Fomalont, E.B.: 1984, *Astrophys. J.* 282, L55

Burns, J.O., Gregory, S.A., Holman, G.D.: 1981, *Astrophys. J.* **250**, 450

Burns, J.O., Gregory, S.A.: 1982, Astron. J. 87, 1245

Burns, J.O., Balonek, T.J.: 1982, Astrophys. J. 263, 546

Burns, J. O., Schwendeman, E., White, R. A.: 1983, *Astrophys. J.* **271**, 575

Cavaliere, A., Fusco-Femiano, R.: 1976, Astron. Astrophys. 49, 137

Colla, G., Fanti, C., Fanti, R., Gioia, I., Lari, C., Lequeux, J., Lucas, R., Ulrich, M.H.: 1975, Astron. Astrophys. Suppl. 20, 1
De Ruiter, H., Parma, P., Fanti, C., Fanti, R.: 1986, Astron. Astrophys. Suppl. 65, 111

Ekers, R.D., Fanti, R., Lari, C., Parma, P.: 1981, Astron. Astrophys. 101, 194

Eilek, J.A., Burns, J.O., O'Dea, C.P., Owen, F.N.: 1984, Astrophys. J. 278, 37

Fanti, R.: 1982, Proc. Astrophysical Jets, eds. Ferrari, A., Pacholczyk, G., p. 253

Fanti, C., Fanti, R., de Ruiter, H.R., Parma, P.: 1986, Astron. Astrophys. Suppl. 65, 145

Fanti, C., Fanti, R., de Ruiter, H.R., Parma, P.: 1987, Astron. Astrophys. Suppl. 69, 57

Fomalont, E.B., Bridle, A.H., Willis, A.G., Perley, R.A.: 1980, *Astrophys. J.* 237, 418

Forman, W., Jones, C., Tucker, W.: 1985, Astrophys. J. 293, 102
Giacconi, R., Branduardi, G., Briel, U., Epstein, A., Fabricant, D., Feigelson, E., Forman, W., Gorenstein, P., Grindlay, J., Gursky, H., Harnden, F.R., Jr., Henry, J.P., Kellogg, E., Koch, D., Murray, S., Schreier, E., Seward, F., Tananbaum, H., Topka, K., van Speybroeck, L., Holt, S.S., Becker, R.H., Boldt, E.A., Serlemitsos, P.J., Clark, G., Canizares, C., Markert, T., Novick, R., Helfand, D., Long, K.: 1979, Astrophys. J. 230, 540

Gorenstein, P., Fabricant, D., Topka, K., Harnden, F.R., Jr.: 1978. Astrophys. J. 224, 718

Harnden, F.R., Fabricant, D.G., Harris, D.E., Schwarz, J.: 1984,Smithsonian Astrophysical Observatory Special Report No. 393

Harris, D.E., Robertson, J.G., Dewdney, P.E., Costain, C.H.: 1982, Astron. Astrophys. 111, 299

- Jaffe, W.H., Perola, G.C.: 1974, Astron. Astrophys. 31, 223 Jones, C., Forman, W.: 1984, Astrophys. J. 276, 38
- Leahy, J. P., Williams, A.G.: 1984, Monthly Notices Roy. Astron. Soc. 210, 929
- Longair, M.S., Seldner, M.: 1979, Monthly Notices Roy. Astron. Soc. 189, 433
- Machalski, J., Condon, J.J.: 1985, Astron. J. 90, 5
- Morganti, R., Fanti, C., Fanti, R., Parma, P., de Ruiter, H.R.: 1987, Astron. Astrophys. 183, 203
- O'Dea, C.P., Owen, F.N.: 1985, Astron. J. 90, 927

- Pacholczyk, A.G.: 1970, Radio Astrophysics, Freeman, San Francisco
- Parma, P., de Ruiter, H.R., Fanti, C., Fanti, R.: 1986, Astron. Astrophys. Suppl. 64, 135
- Parma, P., Fanti, C., Fanti, R., Morganti, R., de Ruiter, H.R.: 1987, Astron. Astrophys. 181, 244
- Perley, R. A., Dreher, J. W., Cowan, J.J.: 1984, *Astrophys. J.* **285**, L35
- Strom, R.G., Fanti, R., Parma, P., Ekers, R.D.: 1983, *Astron. Astrophys.* 122, 305